Analysing the performance of liquid cooling designs in cylindrical lithium-ion batteries

Matthew Yates, Mohammad Akrami *, Akbar A. Javadi

Department of Engineering, College of Engineering, Mathematics, and Physical Sciences, University of Exeter, Exeter, United Kingdom

*Corresponding Author

Dr Mohammad Akrami,

University of Exeter, Exeter, United Kingdom, EX4 4QF

Tel (Fax): +44 1392 724542

Email: m.akrami@exeter.ac.uk

Abstract

The thermal management of batteries for use in electric and hybrid vehicles is vital for safe operation and performance in all climates. Lithium-ion batteries are the focus of the electric vehicle (EV) market due to their high power density and life cycle longevity. To investigate the performance of two liquid cooling designs for lithium-ion battery packs, a series of numerical models were created. The effects of channel number, hole diameter, mass flow rate and inlet locations are investigated on a mini channel-cooled cylinder (MCC) and a channel-cooled heat sink (CCHS); those being the two most efficient concepts. The results show that the maximum temperature can be controlled to under 313K for both designs with mass flow rates over 5E-05 kg/s, and maximum temperature variation can be controlled to less than 3.15K for both designs. Considering both maximum temperature and temperature uniformity, the MCC design provides superior performance to the CCHS. The maximum temperature of the MCC is less than that of the CCHS but the temperature is less uniform. The MCC is a more complex design and so would incur greater manufacturing costs. But, it increases the efficiency of such systems for the rechargeable battery packs of the electric vehicle industry.

Keywords:

Thermal management, Liquid cooled cylinder, Liquid channel cooling, Lithium-ion cells, electric vehicle

Nomenclature

C	cell voltage or cell potential [V]
Cp	heat capacity [$J \cdot kg^{-1} \cdot K^{-1}$]
e	electron
E	open circuit voltage [v]
F	Faraday's constant (96,485 Columb/mol)
k	thermal conductivity [$W \cdot m^{-1} \cdot K^{-1}$]
K	Kelvin
I	discharge of current [A]
n	number of flow of electron
p	pressure
ΔS	battery reaction entropy change [$J.K^{-1}$]
t	Time [s]
T	Temperature [°C or K]
$\vec{v}$	velocity of water [$m.s^{-1}$]
V	operating voltage [v]

Greek symbols

ρ	density (kg/m^3)
∇	divergence
μ	Dynamic fluid viscosity [Pa·s]

Subscripts

a	Aluminium
dif	difference
gen	generation
max	Maximum
w	water

Superscripts

o	Degree

Acronyms

CCHS	channel-cooled heat sink
CFD	Computational Fluid Dynamics
EU	European Union
EV	Electric Vehicle
ICEM-CFD	popular proprietary software package used for CAD and mesh generation
Li	Lithium
MCC	mini channel-cooled cylinder
Ni-MH	Nickel-metal hydride
UDF	user-defined function
USA	United States

1. Introduction

The global issues of energy shortage and pollution have increased the demand for electric and hybrid vehicles [1], with sales projected to rise to 11-15% for all new car sales in the EU and China by 2025, and 16-20% in the USA [2]. The transportation sector currently consumes 49% of the world's oil resources annually and is the most rapidly-growing consumer of global energy [3]. Therefore, it is vital to have green transport solutions for the future. One such solution is hybrid and electric vehicles powered by rechargeable battery packs. Many batteries are available, from lead-acid and nickel-metal hydride (Ni-MH) to lithium-ion [4]. Lithium-ion batteries have the highest power density [5], longest life cycles [6] and lowest self-discharge rates of these battery types [7]. These benefits make lithium-ion batteries the most used powertrain for hybrid and electric vehicles. During operation, lithium-ion battery packs generate a significant amount of heat that needs to be expelled from the pack, which is a major challenge in hybrid and electric vehicles due to the importance of volumetric and gravimetric energy [8]. Temperature has a significant effect on the performance, safety and life cycle of lithium-ion batteries [9], with the ideal operating temperature of lithium-ion batteries found to be between 20-40 ^{o}C [4, 10]. Not only is the maximum operating temperature vital, but the temperature homogeneity of the battery pack is also important, as an uneven temperature distribution can lead to localised deterioration and state of charge mismatches [11]. The desirable temperature distribution in a pack is less than 5 ^{o}C from module-to-module or within a battery [4]. Lithium-ion batteries exceeding the maximum temperature can enter thermal runaway and cause the battery to catch fire or explode [12] with potential physical dangers and replacement costs. It is therefore necessary for thermal management systems to keep the maximum temperature within the desired range of 20-40 ^{o}C and keep the temperature variations within the pack as low as possible. Thus far, different studies have investigated the thermal management [13, 14] using liquid cooling with a flexible channel [15], heat spreader to a liquid-

cooled plate [16] and air cooling [17], however the performance of such models has not been evaluated in detail. The maximum temperature and temperature uniformity will be used to quantify model performances in this study. The gravimetric and volumetric energy, as well as cost and complexity, will be further considered during the process.

2. Model development

The numerical simulations in this paper were developed through Fluent 18.1 and geometries were created in SolidWorks 2016 (Dassault Systèmes, SolidWorks Corp., USA). The purpose of this study is to optimise two liquid cooling methods proposed in (9) and (11) on a concurrent cells format for accurate comparison. Tetrahedral element meshes were created with the use of ICEM Computational Fluid Dynamics (CFD) within Fluent 18.1. The temperature of inlet water and its initial temperatures were assumed to be 298K. Mass flow rate inlet and pressure outlet at atmospheric pressure were selected as inlet and outlet boundary conditions of the fluid. The walls separating gaseous domains, flow domains and solid domains as well as between solid domains were set to coupled walls allowing for natural convection between cells. No slip condition and stationary walls were set for the inside surface of the channels. The module systems were assumed to be in an adiabatic environment as batteries are often located in narrow confined spaces with difficult airflow, and as air is easily heated [18], its thermal effect is negligible. Therefore, the outside surfaces of the module were set as thermally-insulating boundaries to simulate the assumed adiabatic conditions. The laminar flow model was selected as the maximum flow rate under all mass flow produced a Reynolds number less than 2300, which is the condition for laminar flow [19]. The material properties used in this study are shown in Table 1. For increased accuracy, the time step size was set to 1s and the maximum number of iterations per time step was set to 500 to ensure convergence before time step

completion. The system run time was 720 seconds as this was the cells' discharge duration at 5 C [11, 20] to provide the basis for how much power discharge the cells could experience, while C-rate is the measurement of the charge and discharge current with respect to its nominal capacity. The convergence criterion of this study is that the residuals of energy and flow equations respectively are below 1.00E-06 and 1.00E-03.

Table 1. Materials used and their properties. Battery properties are derived from [21], materials from [18].

Material	ρ ($kg \cdot m^{-3}$)	C_p ($J \cdot kg^{-1} \cdot K^{-1}$)	k ($W \cdot m^{-1} \cdot K^{-1}$)	μ ($Pa \cdot s$)
Aluminium	2719	871	202.4	-
Battery	1760	1108	3.91	-
Water	998.2	4128	0.6	1.003×10^{-3}

The temperature of a single cell was calculated by equation 1 [7];

$$\frac{\delta}{\delta t}\left(\rho \cdot C_p \cdot T\right) = \nabla \cdot (k \cdot \nabla T) + Q_{gen} \qquad \text{Equation (1)}$$

Q_{gen} is the heat generation of the battery, ρ is the density of the battery internals, C_p is the heat capacity, k is the thermal conductivity, μ is dynamic fluid viscosity, T is temperature and ∇ · is divergence.

Q_{gen} can be expressed as [7];

$$Q_{gen} = I(E - V) - T\Delta S\frac{I}{nF} \qquad \text{Equation (2)}$$

where I is the discharge of current, E is the open circuit voltage, V is the operating voltage, I is the discharge current, n is the number of flow of electrons, ΔS is the battery reaction entropy change and F is the Faraday constant (96,485 Columb/mol).

Liquid water is used as the coolant in this study, and the continuity equations of water in fluid channels can be expressed by [11]:

$$\frac{\delta \rho_w}{\delta t} + \nabla \cdot (\rho_w \vec{v}) = 0 \qquad \text{Equation (3)}$$

The density of water is ρ_w, and $\vec{v}$ is the velocity of water.

Momentum conservation of the water can be defined as [11]:

$$\frac{\delta}{\delta t}(\rho_w \vec{v}) + \nabla \cdot (\rho_w \vec{v}\vec{v}) = -\nabla p \qquad \text{Equation (4)}$$

where p is the static pressure of water.

Therefore, the energy conservation of water can be defined as [11]:

$$\frac{\delta}{\delta t}(\rho_w c_{pw} T_w) + \nabla \cdot (\rho_w c_{pw} \vec{v} T_w) = -\nabla \cdot (k_w \nabla T_w) \qquad \text{Equation (5)}$$

where c_{pw} is the heat capacity, T_w is the temperature and k_w is the heat capacity of the water.

The energy conservation of the aluminium heat sinks is [7]:

$$\frac{\delta}{\delta t}(\rho_a c_{pa} T_a) = \nabla \cdot (k_w \nabla T_w) \qquad \text{Equation (6)}$$

where ρ_a, c_{pa}, T_a, and k_w are the density, heat capacity, temperature and thermal conductivity of the aluminium heat sinks respectively.

The electrochemical reactions in the anode and the cathode during the charging and discharging processes are shown in equations 7 and 8 [22, 23]:

Anode (a graphitic carbon electrode with a metallic backing):

$$LiC_6 \underset{\text{Charge}}{\overset{\text{Discharge}}{\rightleftharpoons}} Li_{1-x} C_6 + xLi^x + e^- \qquad \text{Equation (7)}$$

Cathode:

$$xLi + xe^- + Li_{1-x}FePO_4 \underset{\text{Charge}}{\overset{\text{Discharge}}{\rightleftharpoons}} LiFePO_4 \qquad \text{Equation (8)}$$

The process is reversible, but batteries lose capacity over time due to electrolyte oxidation damaging electrode surfaces during cycling of the battery. The electrolyte for such batteries is usually ethylene carbonate dimethyl carbonate (EC–DMC) 1-1 lithium perchlorate ($LiClO_4$) 1M [24], while the anode is a hard carbon or sometimes a graphite with intercalated metallic lithium. Cathode's weight is mainly composed of 90% C-$LiFePO_4$, grade Phos-Dev-12, 5% carbon EBN-10-10 (superior graphite) and also 5% polyvinylidene fluoride (PVDF) [25]. The cell considered in this research is a 18650 cylindrical lithium battery at the high power 5 C discharge rate [26]. A simplified numerical model of the NCR18650 battery was created using a solid cylinder with height 65 mm and radius 9.25 mm [27]. Other properties of this battery includes a rated capacity of 2700mAh at 20 °C, nominal voltage of 3.6 V, energy density of 577 Wh/l volumetric and 215 Wh/kg gravimetric. Its charging conditions also based on constant-current and constant voltage (CC-CV) of 1925 mA, 4.20v for 3 hours [25].

The cells' power generation rate is a function of height coordinate value, and this is used to simulate the uneven temperature distribution of cylindrical batteries [11]. The density, thermal conductivity and specific heat capacity of the battery are assumed to be homogeneous across its volume [21] and are set as shown in Table 1. A total element number of 74,350 was assigned since the heat transfer rate only differs by 0.02% when the element number is increased from 74,350 to 286,198, and so with computational power restraints, the lowest element number for accurate results is selected.

2.1. Case 1: Mini Channel Cylinder Creation (MCC)

The first thermal management system proposed is similar to the system suggested in the literature [11] and is adapted for the battery considered in this research. The geometry was

created (see Figure 1) in Solidworks 2016 (Dassault Systèmes, SolidWorks Corp., USA). The battery of 65 mm is covered by a 1 mm thick plate at either end to insulate it from the fluid domain. The channels within the cylinder are equidistantly distributed and, in this study, 2, 4, 6, 8 and 10 channels were considered. Based on the mesh sensitivity study on a singular tube and battery, 98,354 elements were assigned, as increasing the elements from 98,354 to 209,482 produced a difference of only 0.076%. The four-battery cell pack further considered in this research consisted of four tubes, arranged with a minimum gap of 0.5 mm between the tube walls. The inlet and outlet location of flow for the fluid domain as well as mass flow rates of fluid were considered to optimise the design. This design system required one cylinder per cell, and thus a system X cells wide and N cells long has X•N cells and cylinders. The wall thickness of the tubes is the same as in study [10] with the wall treatment of (y^+ = 5) [14].

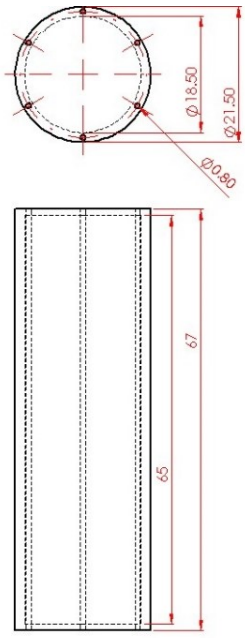

Figure 1. Dimensions of each battery tube.

2.2 Case 2: Channel-Cooled Heat Sink Creation (CCHS)

The second thermal management system proposed is similar to the suggested system [18], in which the surface of the battery is in contact with an aluminium heat sink. This heat sink has fluid channels running through it to extract the heat, and the dimensions of the heat sink part are shown in Figure 2. The numbers of channels considered in this study were 4, 6, 8 and 10, and the radii of these holes were further considered. The number of elements selected per cell and two heat sinks was 110,891, which allowed a two-by-two geometry to be created. The gap between cell centres was assumed to be 22 mm in the X direction and 20 mm in the Z direction, with the heatsinks along a channel line all connected. A fluid domain was assumed to be imposed on the initial and final heat sink faces, and inlet and outlet locations of the fluid domain were considered as well as inlet mass flow rates. This design required a heat sink on either side of the battery to provide a fair simulation of the cooling received by cells within a pack. As downstream batteries were added, connecting heat sinks were added with the downstream requirement of only one additional row of heat sinks for every additional row of cells. A geometry with X downstream cells and N cells wide will have X•N cells and (X+1)•N heat sinks. Therefore, adding cells downflow rather than along the width reduces the number of heat sinks required, but doing so incurs heat transfer problems. This is caused by downstream fluid having a greater temperature than upstream fluid due to heat transfer from heat sinks, thus reducing the heat transfer rate downstream. To balance this effect, the aluminium block of each heat sink downstream is in contact with the relative upstream component in contrast to the design proposed in [11], which has tubes running through each heat sink, as this was found to provide better temperature distribution between cells. The contact between heatsinks provides a further heat transfer medium between the expected hotter cells downstream and those providing the better cooling upstream.

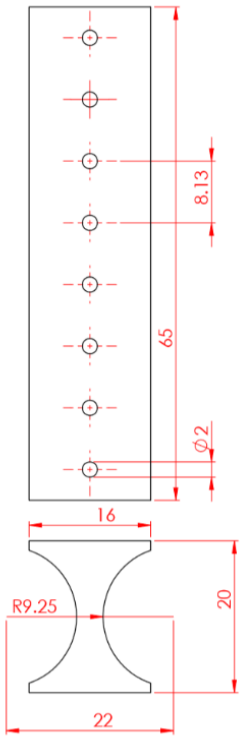

Figure 2. Dimensions of each heat sink

Once each geometry had been created, it was imported into Fluent 18.1. The faces of cell walls, fluid tube walls and inlet and outlet tubes were selected and named selections were created within the sub-program Design Modeller. ICEM CFD was opened within ANSYS Fluent to create a mesh of tetrahedral elements; the mesh was refined using face sizing, and inflation layers at the walls which are critical to heat transfer, such as walls of fluid tubes and cells. Cell zone conditions of the batteries were set to the new material, heat sinks were set to aluminium, and fluid domains were set to liquid water. Inlet and outlet boundary conditions of flow were set along with coupled walls and thermally-insulating walls. Hybrid initiation was used at 100 iterations; the calculation was run with 720-time steps of 1s and a maximum of 500 iterations per time step.

3. Results and discussion

3.1. Results for one singular cell

Previous tests work on 18,650 cells which are based upon the results reported in the literature [20]. The results show that the maximum temperature of the cell at a high power 5 C discharge rate was found to be 351 K after 720 seconds. The average power generation per unit volume of the user-defined function (UDF) source term used in this research was 190,000 W/m^3, producing a cell surface maximum temperature (T_{max}) of 351 K after 720 seconds and cell heat distribution as shown in Figure 3. The temperature values and contours were consistent with the expected maximum temperature at a 5 C discharge in the current literature [20], and with the cell temperature distribution demonstrated in [21]. This validates the simplified numerical battery model used in this study. The model assumes an even power generation rate irrespective of time and temperature, with power generation set as a function of height coordinate with higher power generation in the upper cell (See Figure 3). In this study, we have obtained similar patterns to previous research works. One study suggested a similar heat generation rate at 5 C discharge [28]. Also, as can be observed, the heat generation is different vertically along the battery cell [29].

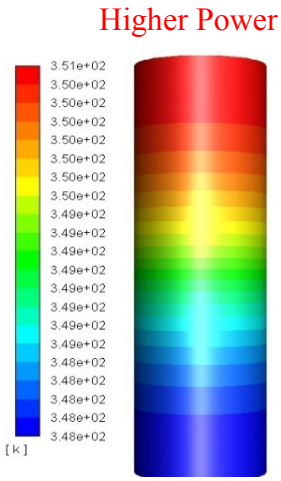

Figure 3. Cell temperature contour after 720s at 5 C discharge

3.2. Results for the Mini Channel-Cooled Cylinder (MCC)

Five different mini channel quantities were compared to study the effect of varying channel numbers. The total mass flow rate of the combined channels was set to 2.5E-05 kg/s for all cases to provide a comprehensive channel effect without a changing mass flow rate affecting the results. Figure 4 shows the evolution of T_{max}, the maximum cell surface temperature, with time for the different number of mini-channels. Initial body temperature and inlet temperature are set to 298K.

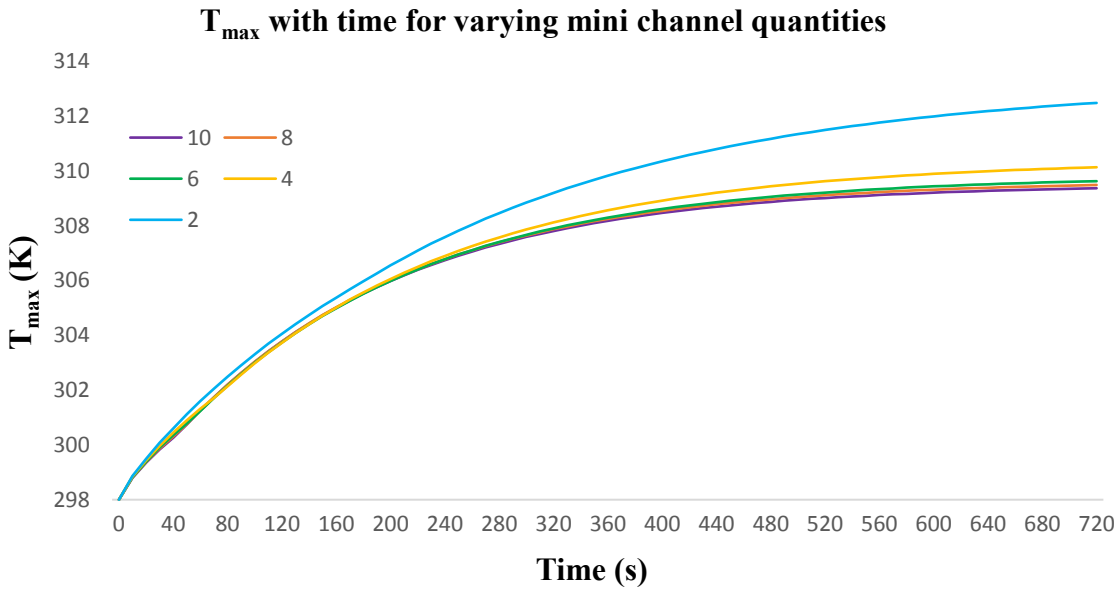

Figure 4. Variation of T_{max} over 720 seconds for different mini channel quantities

For all results, the graph shape of maximum temperature is the same; all results approach an individual asymptote at which point the heat transfer out of the system is equal to the power generation of the system, and thus temperature is constant. The maximum temperature decreases as the number of channels increases, but the change is less significant after 6 channels due to the decreasing distance between the channels. The optimum operating temperature of lithium-ion cells is 293-313 K [4]. In all channel situations, the maximum temperature is within this specified range, but the simulation assumes an idealised consistent flow over all channels, which within a battery pack is likely not the case. The relative performance increase after more than 6 channels is negligible and increased channel quantity increases the complexity of the structure and thus the cost of manufacturing. Therefore, considering cost, complexity and performance, the 6 channel case is to be used further in this study to consider the influence of inlet/outlet location and mass flow rate on a two-by-two cell pack. The maximum cell surface temperature of a single cell under these conditions was found to be 309.63 K, with the inlet location at the cell end having the greatest power generation. The inlet location was reversed, and the maximum temperature was found to be 310.33 K, and so the flow locations further considered will have an inlet from the cell ends of higher power generation.

Besides this, the effect of inlet and outlet locations on the thermal performance within a four cell pack need to be investigated. Six location combinations are considered, and they are shown in Figure 5 and Table 2. The performance of each combination is shown by the maximum temperature after 720s (see Figure 6) and by the difference between maximum and minimum cell surface temperatures (T_{dif}) within the pack (see Table 3). The mass flow rate at the inlet was set to 5E-05 kg/s for all cases and inlet and outlet diameters were set to 4mm.

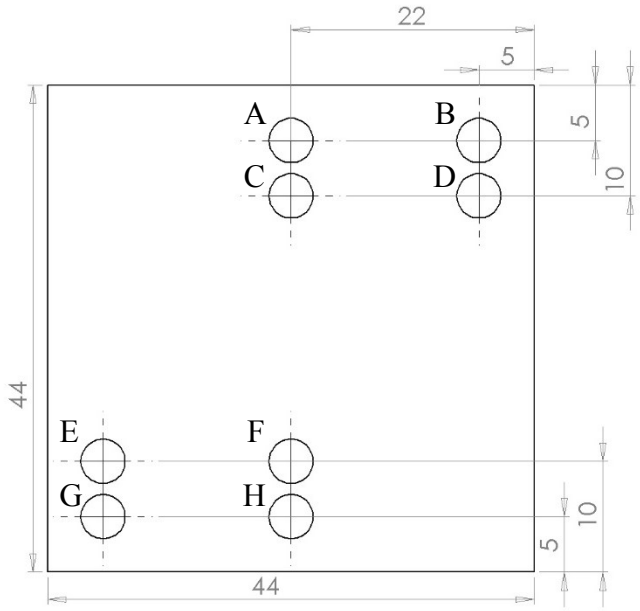

Figure 5. Dimensions of the location combinations, A-D for inlets, E-H for outlets

Table 2. Inlet and Outlet combinations from Figure 4.

Location Combination	Inlet	Outlet
1	A	H
2	C	H
3	C	F
4	B	E
5	D	E
6	B	G

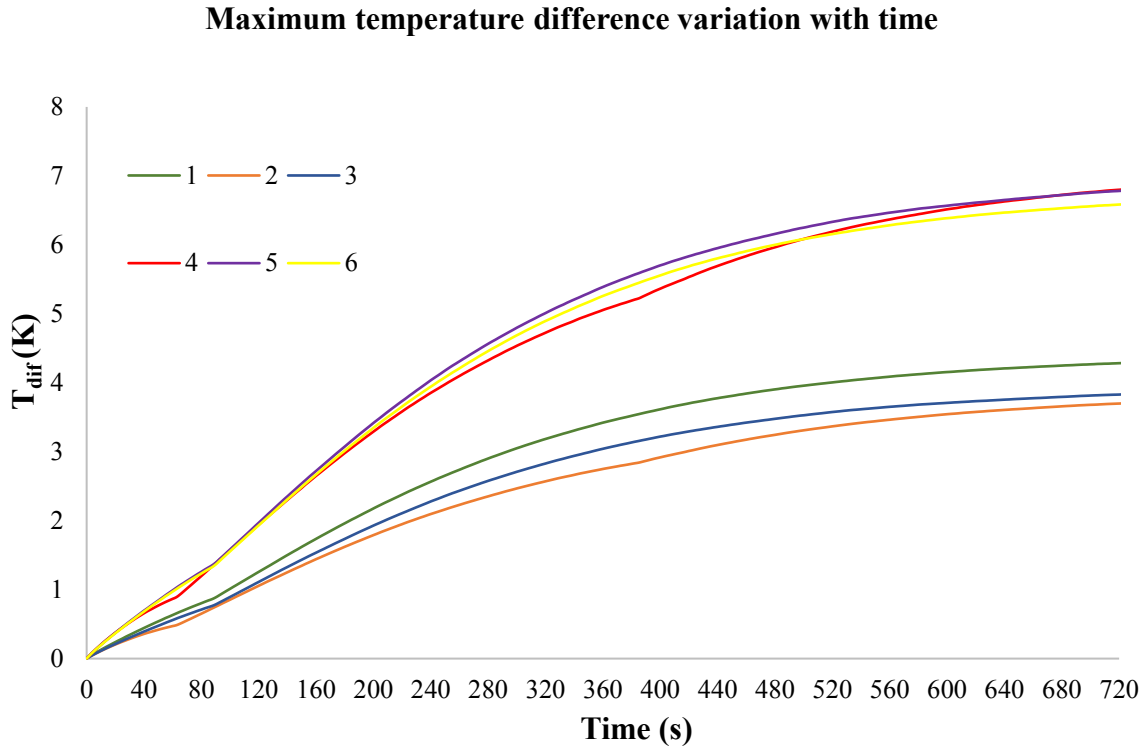

Figure 6. Maximum temperature difference variation with time for the inlet and outlet locations shown in Table 2

Table 3. Maximum temperature and maximum temperature difference at 720s

Locations	T_{max} (K) at 720s	T_{dif} (K) at 720s
1	311.20	4.28
2	311.05	3.75
3	311.19	3.83
4	313.64	6.80
5	314.02	6.78
6	313.74	6.58

The maximum temperature for location combinations 4, 5 and 6 is shown to be significantly higher than that for locations 1, 2 and 3, as is the maximum temperature difference of cell surfaces; this is due to the inlet and outlet locations in 4, 5 and 6 causing the mass flow to be

more unevenly distributed within the structure than combinations 1, 2 and 3. Therefore, locations 4, 5 and 6 will be ignored, as they provide insufficient cooling when compared to the other geometries, as well as significantly greater temperature differences within the pack, which can lead to uneven degradation of cells, which in turn causes issues with state of charge [11]. Location combination 2 is shown to provide the most even temperature distribution within the pack as well as the lowest maximum surface temperature, and so the geometry is to be further considered in this report to study the effect of mass flow rate. Location combination 2 also provided the greatest cooling effect as the system was heated from 0 to 720 seconds.

Five mass flow rates are considered in this study, ranging from 1E-05 to 5E-04 kg/s. The maximum temperature and temperature difference after 720s are shown in Table 4 and the difference between the maximum and minimum temperature within the pack over time is shown in Figure 7.

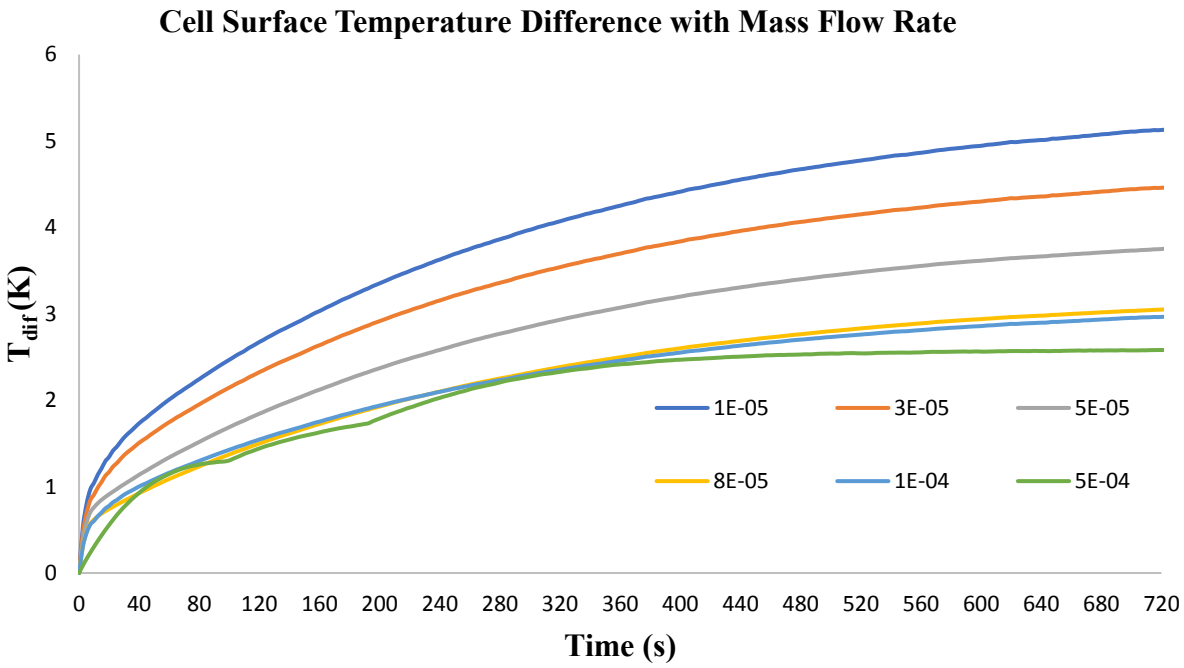

Figure 7. Maximum temperature difference variation with time for varied mass flow rates.

Table 4. Maximum temperature and maximum temperature difference at 720s with changing mass flow rates.

Mass Flow Rate (kg/s)	T_{max} (K) at 720s	T_{dif} (K) at 720s
1.00E-05	318.82	5.12
3.00E-05	314.85	4.46
5.00E-05	311.05	3.75
8.00E-05	310.26	3.05
1.00E-04	310.15	2.96
5.00E-04	309.51	2.58

Mass flow rates of 1E-05 and 3E-05 kg/s do not provide sufficient cooling to keep the maximum temperature within the pack inside the optimal operating temperature of lithium-ion batteries of 313K. The maximum temperature of the pack is not sufficiently reduced beyond the mass flow rate of 8E-05 kg/s and neither is the temperature uniformity of the pack, as shown by Figure 10. The largest mass flow rate considered, 5E-04 kg/s, provided the lowest maximum temperature and most consistent temperature uniformity after 720s. The decrease in temperature difference at a point between 50s and 100s for the 5E-04 kg/s flow rate is put down to computational error caused by increased residual errors from the increased flow rate. This does not influence the final temperature performance of the condition, as the flow stabilises and the result still approaches an asymptote as expected. Increasing the mass flow rate decreases the cell surface maximum temperature within the pack as well as the maximum difference in temperature but at a reduced rate for each increase in flow; this phenomenon is also demonstrated in the study by Zhao et al. [21]. The maximum temperature and maximum temperature difference in this research do not vary with time, as cells' power generation is not set as a function of time, so cells are only asymptotic to their maximum temperature. The

greater the mass flow rate, the greater the power consumption required to generate the flow and thus, the greater power consumption required for the system. Considering the cost, power and performance, the optimal mass flow rate selected was 8E-05 kg/s.

Final optimised MCC design

The final optimised MCC design for the four cell 18650 battery pack considered in this study consists of 6 mini channels per cylindrical cooling tube, with the inlet location set at location 2 from Table 2 and Figure 4 and a mass flow rate of 8E-05 kg/s of water. This produces a maximum cell surface temperature of 310.26K, which is well within the operating temperature of lithium-ion cells.

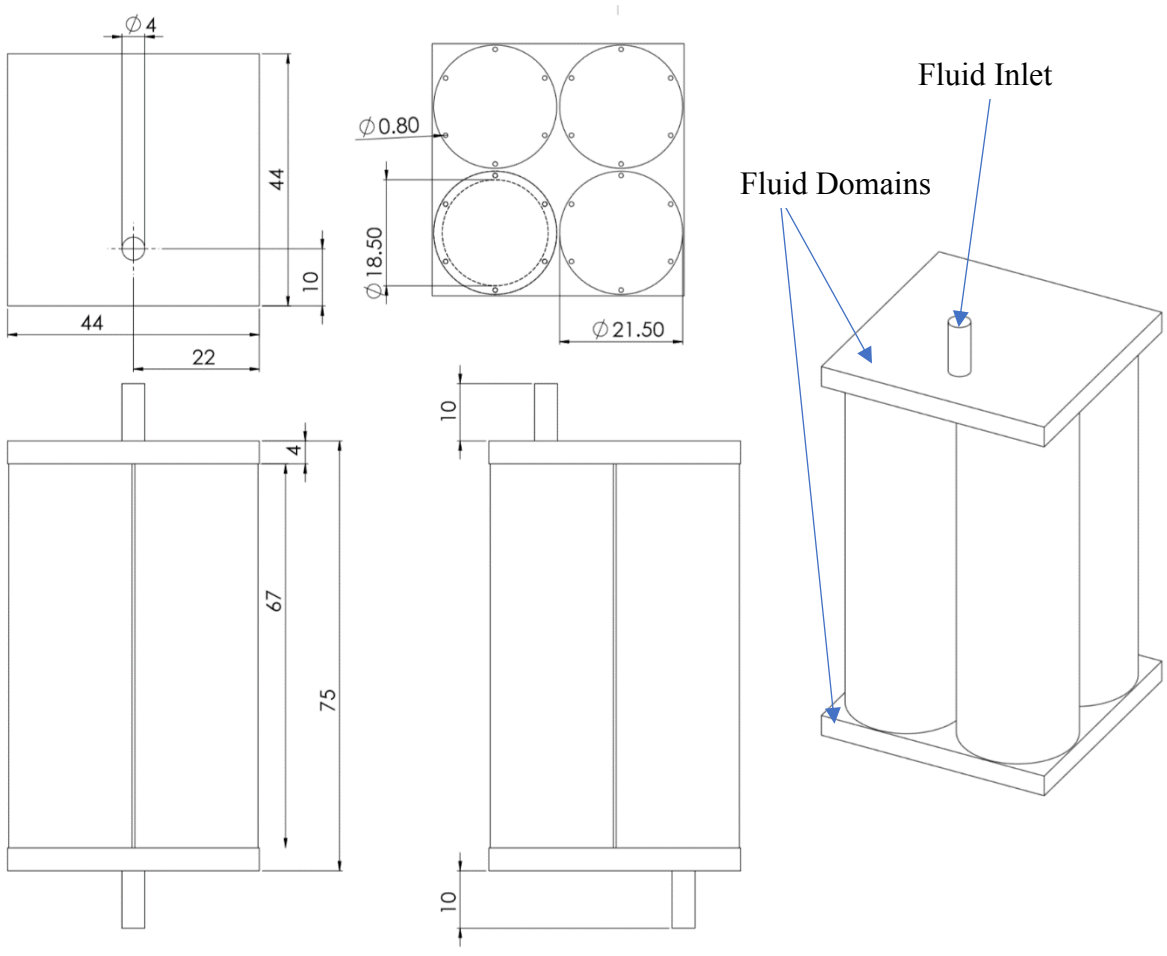

Figure 8. The final design of the MCC, showing the top, side, front views and an isometric view. Inlet tube location is shown along with fluid domain locations.

The maximum temperature difference within the pack is 3.05K and so is also within the suggested 5K target from the current literature [4, 7]. The final design geometry is displayed (see Figure 8) with some basic dimensions and the face of the front battery and tube hidden to show the fluid tubes inside.

3.3. Results for the Channel-Cooled Heat Sink (CCHS)

Battery heat generation is transferred to heat in the heat sink by conduction, and heat is then removed by water channels along its length. Four options were reviewed, with 4, 6, 8, 10 and 12 channels being investigated. The maximum cell surface temperature after 400s and after 720s under the different input parameters is shown (see Table 5). The total mass flow rate of the combined channels was set to 2.5E-05 kg/s for all scenarios, and each hole was set to have a radius of 1 mm and to be evenly distributed vertically within the heat sink.

Table 5. T_{max} at 400s and 720s of the cell surface with different fluid hole quantities.

Numbers of Channels	T_{max} (K) at 400s	T_{max} (K) at 720s
4	307.67	310.70
6	307.72	310.62
8	307.46	310.46
10	307.41	310.43
12	307.41	310.41

The temperature at both 400s and 720s is similar across all results, as shown in Table 5, due to the large conduction surface of the heat sink connected to the aluminium battery, which has a high thermal conductivity, allowing for quick heat transfer [30]. The number of holes chosen for the remainder of this study was 8 as this provided an optimal between the overall cooling effect and cost, as a design with more holes is more complex and therefore more expensive.

The diameter of the holes was also varied to create a more even temperature distribution within the cell due to its uneven power generation. The diameter of the upper four (higher power generation end shown in Figure 3) and lower four holes (lower power end) were varied to achieve this effect. The diameters investigated all maintained the same channel volume to ensure the volume of the heat sink was not affected. The mass flow rate inlet was again set to 2.5E-05 kg/s and the upper four holes increased in diameter and the lower four decreased. The results are shown in Table 6.

Table 6. Cell surface T_{max} maximum ΔT at 720 seconds with different hole diameters.

Hole Diameter (mm)		Cell surface T_{max} at 720s (K)	Max T_{dif} at 720s (K)
Upper four holes	Lower four holes		
2	2	310.44	1.52
2.18	1.8	310.11	0.44
2.34	1.6	310.09	0.39
2.46	1.4	310.18	0.39

The maximum cell surface temperature decreases as the upper holes are increased in size and the lower four are decreased until an upper diameter 2.46mm. At this point, the fluid velocity within the top holes is decreased significantly so that the fluid within the tubes has equalised in temperature before reaching the outlet, and thus does not remove heat as efficiently [31].

A two-by-two cell geometry with 6 heat sinks (three-by-two) was created to study the effects of mass flow rate and inlet location. The cell temperature was still greater in the upper region, so inlet locations are considered from this end, passing through the 4 cells at the lower geometries shown in Figure 9 and Table 7. The mass flow inlet was set to a flow of 1E-04 kg/s

for all scenarios and inlet and outlet diameters were set to 5mm. The results are shown in Table 8 for T_{max} and max T_{dif} at 720 seconds.

Table 7. Inlet and outlet combinations.

Location Combination	Inlet	Outlet
1	I	N
2	K	N
3	K	L
4	I	L
5	J	M

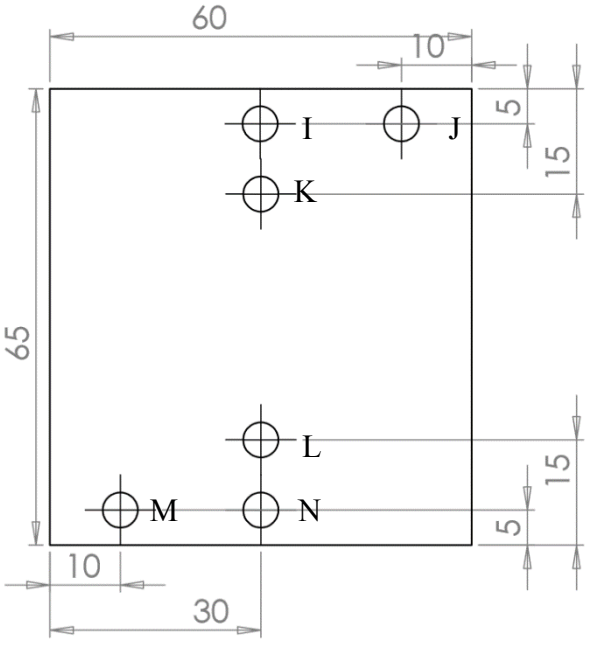

Figure 9. Inlet locations from I-K and outlet locations from L-N. Outlet locations are on a second fluid domain behind the cells. The fluid domain is 60mm wide and 65mm in height, which is the height of the batteries.

Table 8. T_{max} and max T_{dif} after 720 seconds for the geometry locations.

Location combination	T_{max} (K) at 720s	ΔT (K) at 720s
1	310.98	1.90
2	311.04	1.91
3	311.13	1.97
4	311.06	1.92
5	314.90	4.09

Location combination 5 provided the worst cooling performance and temperature uniformity due to their positions causing greater flow over the right cells in the pack than the left, which in turn created a larger temperature difference. The remaining locations provided little difference to the overall effect on cell surface temperature due to the heat sink allowing for even temperature distribution within the pack. However, location combination 1 did provide both the optimal cooling and the most even temperature distribution in the pack and so was selected as the location to be used in this research to analyse the effect of mass flow rate. Location combination 1 has the inlet and outlet evenly spaced horizontally within the fluid domain and the inlet and outlet 5 mm from the top and bottom of the domain respectively.

In this part, four mass flow rates are considered in this study, ranging from 5E-05 to 2E-04 kg/s, with the maximum cell surface temperature and the maximum difference in cell surface temperature shown in Figure 10 and Table 9 respectively.

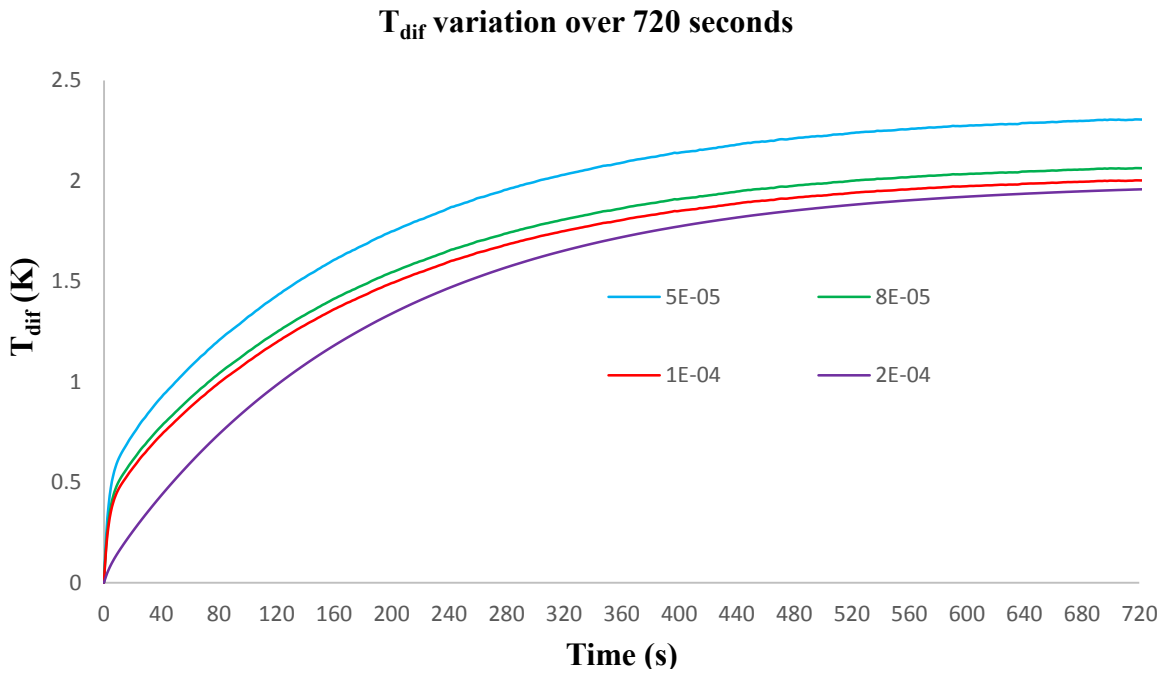

Figure 10. Maximum temperature difference variation with time for varied flow rates

Table 9. T_{max} and T_{dif} after 720 seconds for flow rates from 5E-5 to 2E-4 kg/s

Flow Rate (kg/s)	T_{max} at 720s	T_{dif} at 720s
5.00E-05	315.83	2.31
8.00E-05	312.19	2.06
1.00E-04	311.01	2.00
2.00E-04	310.88	1.96

The maximum temperature and temperature difference decrease with increasing flow rate, as seen in Table 9, and there is a significant change from 5E-05 to 8E-05 kg/s with a decrease of over 3K in maximum temperature. The maximum temperature difference for 2E-4 kg/s, the fastest flow, is significantly lower than that for 1E-04 and 8E-05 kg/s for the majority of the flow, but approaches an asymptote not significantly different, and so its increased power usage

fails to provide a long-term cooling difference, as further shown by the similar values of T_{max} in table 9 for 1E-04 and 2E-04 kg/s. Mass flow rate of 1E-04 kg/s provides over 1K more cooling than 8E-05 kg/s and little benefit is gained from the increase to 2E-04 kg/s, and thus 1E-04 kg/s is selected as the optimum flow rate.

Final optimised CCHS design

The final CCHS design consisted of eight horizontal channels, the upper four of which had a diameter of 2.34 mm and the lower four 1.6 mm. The inlet/outlet locations from Table 1 is location combination 1. The optimal mass flow rate tradeoff was selected as 1E-04 kg/s, which produced a maximum cell surface temperature of 311.01K and a maximum surface temperature difference of 2.00K. This is within the optimal operating range of lithium-ion batteries of 313k and provides a good cell-to-cell temperature distribution, which is important to overall pack performance, as at high temperatures the performance of a pack is limited by the hottest cell [32]. The final geometry of the CCHS is shown in Figure 10, with the nearest heat sink set to transparent to show the fluid tubes within. The outlet is shown at the top of the display and is located closer to the fluid tube holes of a smaller diameter to improve the temperature uniformity performance of the system, as shown in Table 6. This number of cells plus one heat sink is required to provide cooling to both sides of each cell, but this will be of more negligible effect in bigger geometries than the four cell geometry of Figure 11.

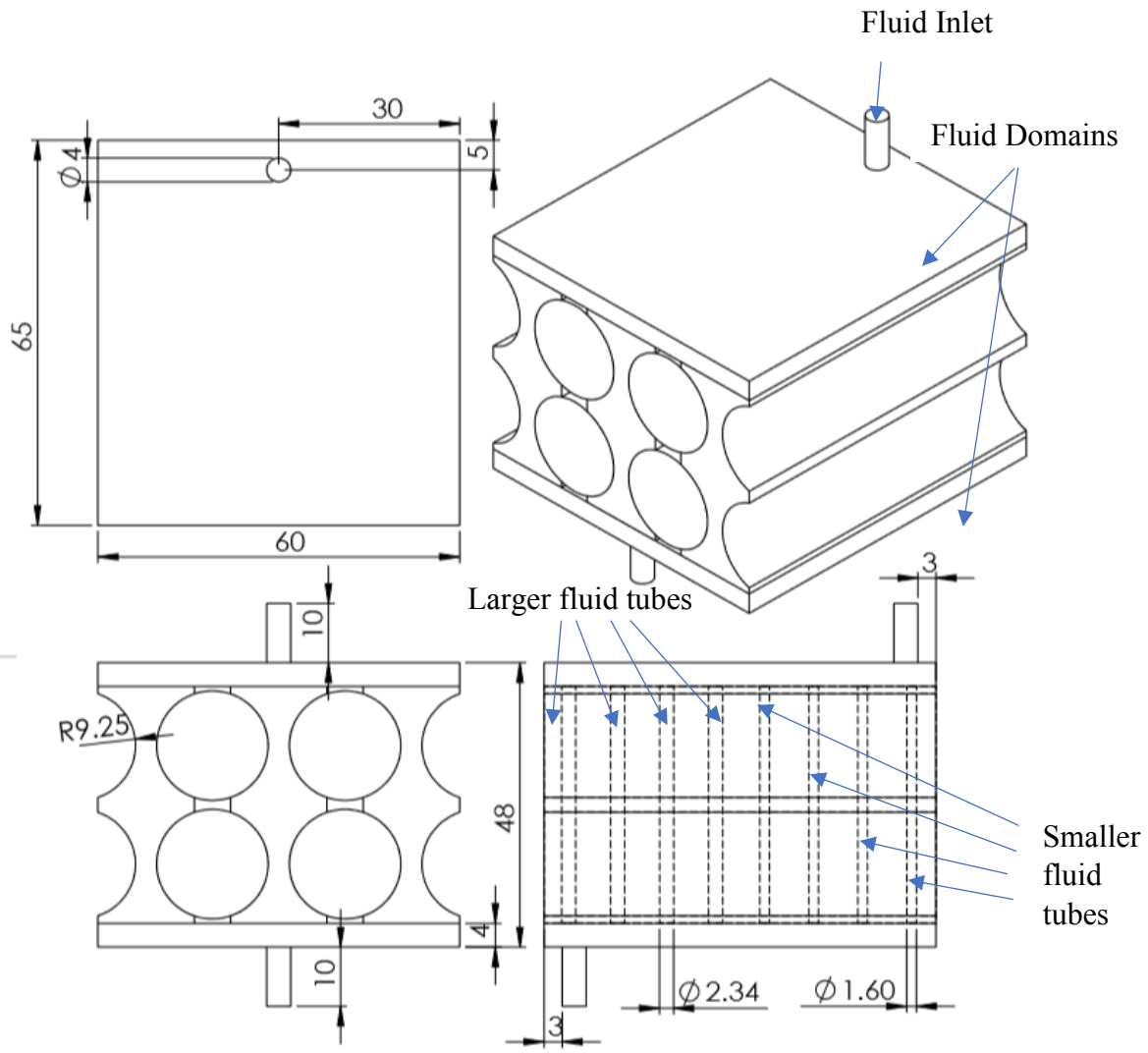

Figure 11. The final design of the CCHS, showing the top, side, front view and an isometric view. Inlet tube dimensions are shown along with fluid domain locations, and the increased fluid tube diameters.

3.4. Comparison of design performances

The two designs are now compared on their relative performance. Figure 12 depicts the variation in maximum and minimum temperature over 720 seconds. The performance is judged by the maximum cell surface temperature to which the cooling system limits the four cell geometry, as well as the uniformity of temperature within the geometry. The weight and

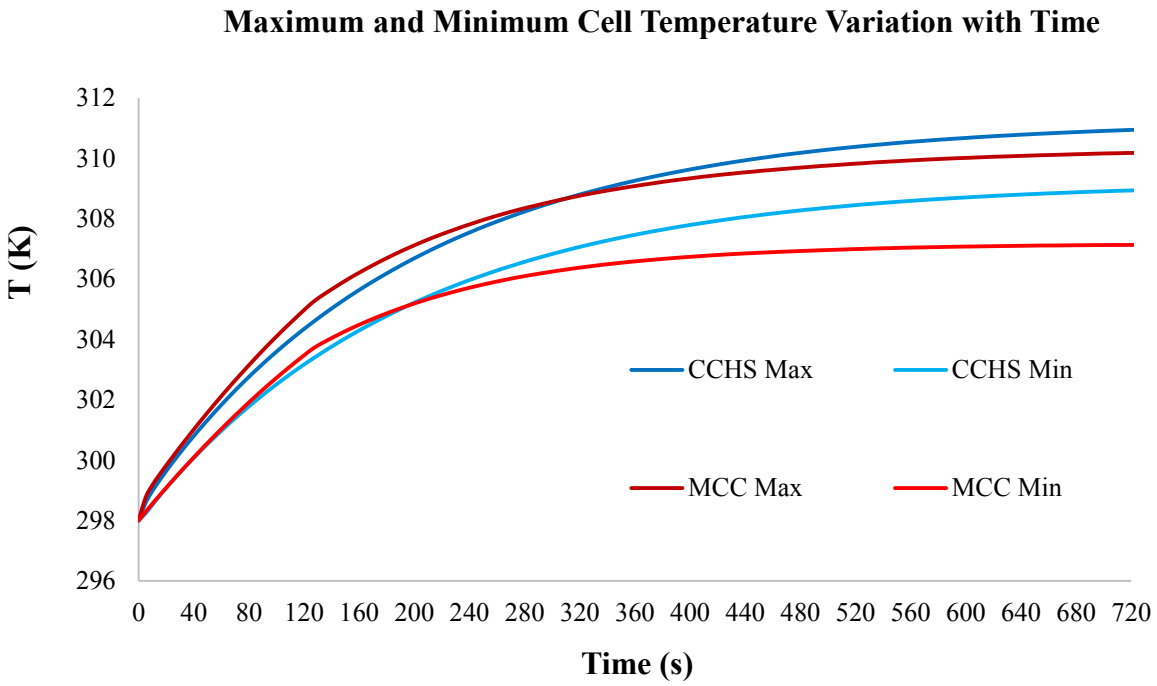

Figure 12. Maximum and minimum cell surface temperatures during the 720 second cycle.

volume of each design are also taken into consideration, as they are vitally important in automotive applications [8].

The MCC provides a superior cooling effect compared to the CCHS, as shown in Figure 12. The maximum and minimum temperature within the four cell geometry are lower for the MCC. The minimum temperature of the CCHS is initially lower than that of the MCC due to the larger size of the heat sink, meaning that more energy is required to raise the temperature of the CCHS system. With both systems having the same power generation, the CCHS is therefore heated more slowly. The MCC provides better heat removal; this is shown by the lower maximum and

minimum temperatures for the system after 720 seconds, which is the runtime for this study. The maximum temperature of MCC was 310.26K (0.75K below the maximum temperature of the CCHS). The minimum temperatures were 307.21K and 309.01K for the MCC and CCHS respectively, and further show the greater cooling power of the MCC. The maximum temperature of the CCHS was 311.01k, and the maximum difference was 2.00k, which was significantly less than the temperature difference of the MCC.

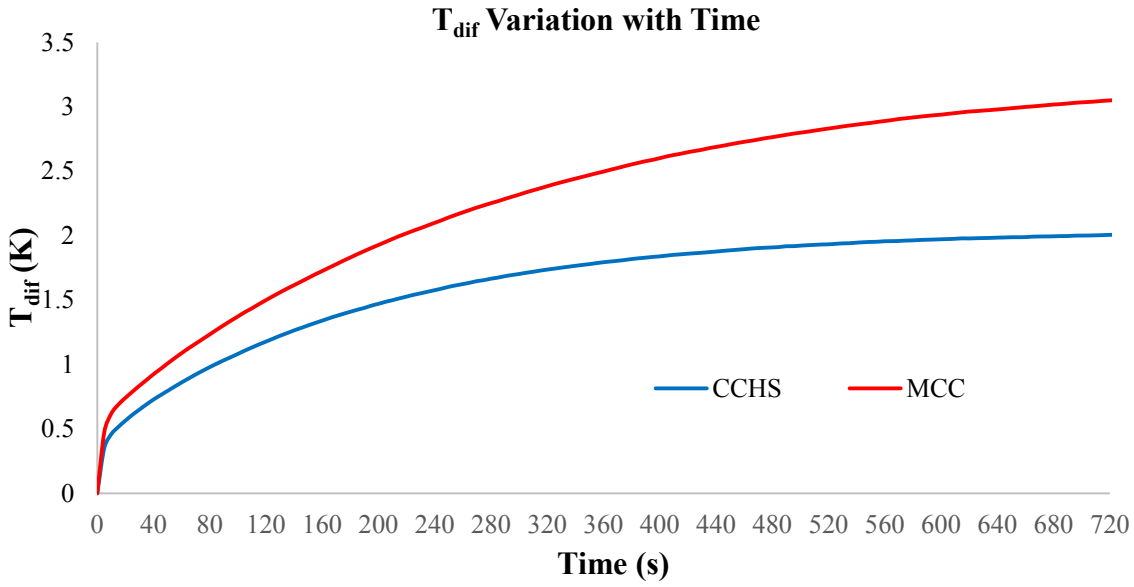

Figure 13. T_{dif} during the 720 second cycle for the optimal CCHS and MCC.

The variation of temperature difference over the 720 second run time is illustrated (Figure 13) and as shown, assuming the same amount of flow rate, the CCHS provides a more even temperature distribution within the cells than the MCC due to the larger volume of its aluminium heat sink. The heat sink is further interconnected between cells on the same flow stream and this allows for a further heat transfer mechanism between cells of uneven temperature distribution. The MCC has a maximum temperature difference of 3.05K, which is 1.05K higher than the CCHS's 2.00K; both of these results are well inside the 5K limit suggested in the current literature [7]. The fact that both results provide such even temperature distributions is due to the small geometry of the battery packs considered in this research due

to the mesh size limitations. The MCC system provides better cooling than the CCHS system, but this comes at the cost of increased temperature difference within the pack. The MCC system is also far more complex than the CCHS system, with 24 cooling tubes of 0.8 mm diameter in the four cell system compared to the 16.2 mm tubes required in the CCHS. The CCHS will also be less complex when enlarged, as downstream cells do not add cooling tubes, but only extend the length of existing tubes. This means the CCHS is a cheaper solution to manufacture due to its less complex geometry and reduced precision of cut required. The heat flux out of both systems after 720 seconds is 13.25W and 13.24W for the MCC and CCHS respectively, and this matches the power generation rate of the batteries (13.28W) to within 0.3%. The power generation average of the batteries is 190,000 W/m^3 over the 6.9889 m^{-3} in the four cell pack, and validates the final results of this study.

The MCC four cell system is made of 26600.84 mm^3 of aluminium, giving it a weight of 72.3 grams without the batteries. Cells in the MCC can only be located every 22 mm in both the x and z-direction (length and height) and with a height of 67 mm, the system requires 32,428 mm^3 per cell. The CCHS requires 59456.30 mm^3 of aluminium, giving it a weight without batteries of 161.7 grams, significantly heavier than the MCC. Cells in the CCHS can be located every 22 mm in the x-direction (length) and 20 mm in the z-direction (height), with the height of 65 mm, and this means the CCHS requires a volume of 28,600 mm^3 per cell, with the weight of each cell being 30.75 grams (see Table 10).

Table 10. The weight of each four cell system, including batteries, fluids and module materials in total and per cell, as well as the volume of space required for the system in total and on a cell basis.

System	Total weight (g) including cells	Weight per cell (g)	Total Volume of space required (mm^3)	Volume Required per cell (mm^3)
MCC	195.3	48.8	129,712	32,428
CCHS	284.7	71.2	114,400	28,600

The MCC system is shown to be over 1.46 times more gravimetrically powerful in terms of cell energy production than the CCHS system, but the CCHS system is 1.13 times more volumetrically powerful. The MCC system provides greater cooling than the CCHS, but this comes at the cost of increased volume and costs due to the complexity of the design, and the smaller dimensions required mean more precision is necessary in the manufacturing process. The CCHS system also provides a greater temperature uniformity within the cell system, but this is achieved at a higher temperature, as shown by the minimum and maximum temperature after 720s being greater (see Figure 12) than the respective MCC values. The complexity and precision required for the MCC design make its use limited to only the most expensive of applications, where its maximal cooling benefits are required. The CCHS is a simpler, less expensive design. It has less effective cooling than the MCC, but has more uniform temperature distribution across the pack.

4. Conclusions

Two liquid water cooling solutions for lithium-ion battery packs were designed and compared in this study. The battery used was a 18650 lithium-ion cylindrical battery at a 5 C discharge rate, and the ambient air temperature assumed was 298K. The influence of channel number, inlet and outlet locations as well as mass flow rate on cooling performance in terms of maximum temperature and temperature distribution were investigated. The size of the cooling channels was also investigated for the CCHC design, and the main conclusions are as follows:

- Increasing the number of channels decreases the maximum temperature of the cell, but with a reducing effect for each increase. It was not necessary to use more than six channels per cell for the MCC and eight for the CCHS, as the benefits beyond these numbers are insignificant.
- As the mass flow rate is increases, the maximum temperature and difference in temperature decreases. The optimal cooling performance was found when the inlet was located nearest to the battery end, which produced greater heat in adiabatic conditions.
- The optimal MCC design has a maximum temperature of 310.26K and temperature difference of 3.05K, which are within the 313K and 5K limits advised for lithium-ion batteries [7]. The number of channels selected is six per tube, with a mass flow rate of 8E-05.
- The optimal CCHS design has eight channels, with mass flow rate into the system of 1E-04 kg/s; this limits the maximum cell temperature to 311.01K and the maximum temperature difference is just 2.00K.
- The MCC design provides better cooling than the CCHS design and is significantly lighter, but this comes at the expense of temperature distribution and increased the complexity of the design, thus limiting its potential use from an economic point of view.

The battery in this study was assumed to be of constant power generation across time and temperature, and its material properties were also assumed to be homogeneous across its volume, which represents a simplified adaptation of real battery characteristics [20] and is a limitation of this research. Future work could analyse the performance of the designs proposed on larger geometries and further, look at the effects of different ambient temperatures on the systems.

Funding

This research did not receive any specific grant from funding agencies in the public, commercial, or not-for-profit sectors.

Declarations of interest

None

Acknowledgement

The authors would like to appreciate the anonymous reviewers for their insightful comments and suggestions.

References

1. Thomas, C.S., *Transportation options in a carbon-constrained world: Hybrids, plug-in hybrids, biofuels, fuel cell electric vehicles, and battery electric vehicles.* International Journal of hydrogen energy, 2009. **34**(23): p. 9279-9296.
2. Worwood, D., Q. Kellner, M. Wojtala, W. Widanage, R. McGlen, D. Greenwood, and J. Marco, *A new approach to the internal thermal management of cylindrical battery cells for automotive applications.* Journal of Power Sources, 2017. **346**: p. 151-166.
3. Amjad, S., S. Neelakrishnan, and R. Rudramoorthy, *Review of design considerations and technological challenges for successful development and deployment of plug-in*

hybrid electric vehicles. Renewable and Sustainable Energy Reviews, 2010. **14**(3): p. 1104-1110.

4. Rao, Z. and S. Wang, *A review of power battery thermal energy management.* Renewable and Sustainable Energy Reviews, 2011. **15**(9): p. 4554-4571.
5. Choi, J.W. and D. Aurbach, *Promise and reality of post-lithium-ion batteries with high energy densities.* Nature Reviews Materials, 2016. **1**(4): p. 16013.
6. Sarre, G., P. Blanchard, and M. Broussely, *Aging of lithium-ion batteries.* Journal of power sources, 2004. **127**(1-2): p. 65-71.
7. Qian, Z., Y. Li, and Z. Rao, *Thermal performance of lithium-ion battery thermal management system by using mini-channel cooling.* Energy Conversion and Management, 2016. **126**: p. 622-631.
8. Chen, D., J. Jiang, G.-H. Kim, C. Yang, and A. Pesaran, *Comparison of different cooling methods for lithium ion battery cells.* Applied Thermal Engineering, 2016. **94**: p. 846-854.
9. Leng, F., C.M. Tan, and M. Pecht, *Effect of Temperature on the Aging rate of Li Ion Battery Operating above Room Temperature.* Scientific Reports, 2015. **5**: p. 12967.
10. Rahman, M.M., H. Rahman, T. Mahlia, and J. Sheng. *Liquid cooled plate heat exchanger for battery cooling of an electric vehicle (EV)*. in *IOP Conference Series: Earth and Environmental Science*. 2016. IOP Publishing.
11. Zhao, J., Z. Rao, and Y. Li, *Thermal performance of mini-channel liquid cooled cylinder based battery thermal management for cylindrical lithium-ion power battery.* Energy conversion and management, 2015. **103**: p. 157-165.
12. Liu, Z., Y. Wang, J. Zhang, and Z. Liu, *Shortcut computation for the thermal management of a large air-cooled battery pack.* Applied Thermal Engineering, 2014. **66**(1-2): p. 445-452.

13. Xia, G., L. Cao, and G. Bi, *A review on battery thermal management in electric vehicle application.* Journal of Power Sources, 2017. **367**: p. 90-105.

14. Panchal, S., R. Khasow, I. Dincer, M. Agelin-Chaab, R. Fraser, and M. Fowler, *Thermal design and simulation of mini-channel cold plate for water cooled large sized prismatic lithium-ion battery.* Applied Thermal Engineering, 2017. **122**: p. 80-90.

15. Zhao, C., W. Cao, T. Dong, and F. Jiang, *Thermal behavior study of discharging/charging cylindrical lithium-ion battery module cooled by channeled liquid flow.* International Journal of Heat and Mass Transfer, 2018. **120**: p. 751-762.

16. Basu, S., K.S. Hariharan, S.M. Kolake, T. Song, D.K. Sohn, and T. Yeo, *Coupled electrochemical thermal modelling of a novel Li-ion battery pack thermal management system.* Applied Energy, 2016. **181**: p. 1-13.

17. Saw, L.H., Y. Ye, A.A. Tay, W.T. Chong, S.H. Kuan, and M.C. Yew, *Computational fluid dynamic and thermal analysis of Lithium-ion battery pack with air cooling.* Applied energy, 2016. **177**: p. 783-792.

18. Rao, Z., Z. Qian, Y. Kuang, and Y. Li, *Thermal performance of liquid cooling based thermal management system for cylindrical lithium-ion battery module with variable contact surface.* Applied Thermal Engineering, 2017. **123**: p. 1514-1522.

19. Aghabozorg, M.H., A. Rashidi, and S. Mohammadi, *Experimental investigation of heat transfer enhancement of Fe2O3-CNT/water magnetic nanofluids under laminar, transient and turbulent flow inside a horizontal shell and tube heat exchanger.* Experimental Thermal and Fluid Science, 2016. **72**: p. 182-189.

20. Wang, Z., X. Li, G. Zhang, Y. Lv, C. Wang, F. He, C. Yang, and C. Yang, *Thermal management investigation for lithium-ion battery module with different phase change materials.* RSC Advances, 2017. **7**(68): p. 42909-42918.

21. Zhao, J., Z. Rao, Y. Huo, X. Liu, and Y. Li, *Thermal management of cylindrical power battery module for extending the life of new energy electric vehicles.* Applied thermal engineering, 2015. **85**: p. 33-43.

22. Mohammadian, S.K. and Y. Zhang, *Thermal management optimization of an air-cooled Li-ion battery module using pin-fin heat sinks for hybrid electric vehicles.* Journal of Power Sources, 2015. **273**: p. 431-439.

23. Saw, L., Y. Ye, and A. Tay, *Electrochemical–thermal analysis of 18650 Lithium Iron Phosphate cell.* Energy Conversion and Management, 2013. **75**: p. 162-174.

24. Klassen, B., R. Aroca, M. Nazri, and G.A. Nazri, *Raman Spectra and Transport Properties of Lithium Perchlorate in Ethylene Carbonate Based Binary Solvent Systems for Lithium Batteries.* The Journal of Physical Chemistry B, 1998. **102**(24): p. 4795-4801.

25. Amine, K., J. Liu, and I. Belharouak, *High-temperature storage and cycling of C-LiFePO4/graphite Li-ion cells.* Electrochemistry communications, 2005. **7**(7): p. 669-673.

26. Panchal, S., M. Mathew, R. Fraser, and M. Fowler, *Electrochemical thermal modeling and experimental measurements of 18650 cylindrical lithium-ion battery during discharge cycle for an EV.* Applied Thermal Engineering, 2018. **135**: p. 123-132.

27. Panasonic NCR18650. (2012). 13th ed. p.1. Available at:https://engineering.tamu.edu/media/4247819/ds-battery-panasonic-18650ncr.pdf, P.N.t.e.p.A.a.

28. Inui, Y., Y. Kobayashi, Y. Watanabe, Y. Watase, and Y. Kitamura, *Simulation of temperature distribution in cylindrical and prismatic lithium ion secondary batteries.* Energy Conversion and Management, 2007. **48**(7): p. 2103-2109.

29. Jeon, D.H. and S.M. Baek, *Thermal modeling of cylindrical lithium ion battery during discharge cycle.* Energy Conversion and Management, 2011. **52**(8-9): p. 2973-2981.

30. Parker, W., R. Jenkins, C. Butler, and G. Abbott, *Flash method of determining thermal diffusivity, heat capacity, and thermal conductivity.* Journal of applied physics, 1961. **32**(9): p. 1679-1684.

31. Sabharwall, P., V. Utgikar, and F. Gunnerson, *Effect of Mass Flow Rate on the Convective Heat Transfer Coefficient: Analysis for Constant Velocity and Constant Area Case.* Nuclear Technology, 2009. **166**(2): p. 197-200.

32. Shahid, S. and M. Agelin-Chaab, *Analysis of Cooling Effectiveness and Temperature Uniformity in a Battery Pack for Cylindrical Batteries.* Energies, 2017. **10**(8): p. 1157.